Eur. Phys. J. A **11**, 285–296 (2001)

THE EUROPEAN PHYSICAL JOURNAL A

Fragmentation of relativistic oxygen nuclei in interactions with a proton

V.V. Glagolev[1,2], K.G. Gulamov[1], V.D. Lipin[1], S.L. Lutpullaev[1], K. Olimov[1,a], Kh.K. Olimov[1], A.A. Yuldashev[1], and B.S. Yuldashev[1,3]

[1] Physical-technical institute of SPA "Physics-Sun" of Uzbek Academy of Sciences G. Mavlyanova str., 2^B, Tashkent, 700084, Uzbekistan
[2] Joint Institute for Nuclear Research, Dubna, Moscow region, 141980, Russia
[3] Institute of Nuclear Physics, Uzbek Academy of Sciences pos. Ulughbek, Tashkent, 702132, Republic of Uzbekistan

Received: 9 January 2001 / Revised version: 6 June 2001
Communicated by W.F. Henning

Abstract. The data on investigation of inelastic interactions of ^{16}O nuclei in a hydrogen bubble chamber at an incident momentum of 3.25 A GeV/c are presented. Separate characteristics as fragments isotope composition and topological cross-sections of fragmentation channels are given. The processes of formation of light fragments and unstable nuclei, and the break-up of the ^{16}O nucleus into multicharge fragments are investigated. A comparison between the experimental data and the calculations of the cascade fragmentation evaporation model (CFEM) is made. The observed singularities of the interactions point out the important role of the nucleus α-cluster structure in the formation of the final products.

PACS. 25.10.+s Nuclear reactions involving few-nucleon systems

1 Introduction

The fragmentation of excited atomic nuclei formed in hadron and hadron-nuclear interactions is one of the fundamental problems in nuclear physics. Experimental data show that at intermediate energies (several GeV per nucleon) fragmentation gives the main contribution to the multiplicity of secondary particles [1,2]. A number of experimental and theoretical works have been devoted to the investigation of this phenomenon. But the full comprehension of this phenomenon does not exist yet, and the existing model calculations are able to depict only some details of this [3,4]. The difficulties in the analysis of the experimental data are firstly caused by the fact that the fragmentation of the atomic nucleus is a mixture of several mechanisms whose role changes depending on the collision energy [4], mass [5,6], and fragmenting nucleus structure [7]. Let us point out also that most of such experiments with production of many fragments belong to interactions with heavy nuclei, where it is difficult to completely reconstruct the structure of the final states. When a large number of projectile fragments is produced in a nuclear reaction, exclusive measurements are necessary to determine the extent of multiple fragmentation and its interrelations with the production of new particles. These experiments are easier to perform in the case of light projectile nuclei (see, *e.g.*, [8]).

[a] e-mail: olimov@physic.uzsci.net

The new experimental results presented in this paper are part of an investigation on the fragmentation of the oxygen nucleus in interactions with a proton at 3.25 A GeV/c momentum. It should be noted that our experiment with relativistic oxygen nuclei as projectiles allows one to investigate in details different fragmentation channels as well as the topology and characteristics of the produced particles (mostly pions).

The experiment was produced under 4π geometry conditions with identification of all secondary charged particles. The data on fragments isotope composition, final-state topological cross-sections, α-particles and light-(^{1}H, ^{2}H, ^{3}H and ^{3}He) fragments characteristics, cross-sections of the short-lived nuclei formation at break-up of oxygen nucleus into multicharge fragments are given.

The data of this paper are based on an analysis of more than 11000 measurements of ^{16}O-p interactions at 3.25 A GeV/c momentum. The experimental results were systematically compared with the predictions of CFEM (cascade fragmentation evaporation model) developed for proton-nucleus reactions at intermediate energies [9]. In the framework of CFEM, the interaction process consists of a couple of stages. First, the stage of intranuclear cascading and second the stage of de-excitation of hot nuclei, with the formation of fragments. For light nuclei, like ^{16}O, the Fermi break-up was used as dominating mechanism of fragment formation. In addition, in the model the contribution of ^{5}He, ^{5}Li, ^{8}Be and ^{9}B unstable nuclei [10] decays

into the final state was also taken into account. For the purposes of the present paper more than 22000 events were simulated.

2 The experiment

The experimental data reported here were collected with a 1 m hydrogen bubble chamber exposed to a beam of oxygen nuclei at a momentum of 3.25 GeV/c per nucleon at the JINR synchrophasotron. Details of the experimental set-up have been published previously [11–14].

The usage of accelerated nuclear beams impinging on the fixed proton target caused all fragments of the incoming nucleus to be fast in the laboratory frame and thus one could well measure and identify them practically without losses. On the other hand, almost all the losses due to the chamber threshold momentum are concentrated in the elastic scattering channels. The ionisation of the charged secondary particles has been estimated visually. The homogeneity and low hydrogen density allowed us to identify with high precision the bulk of charged secondaries on the basis of ionisation and produced measurements.

Pictures of ^{16}O-p interactions were scanned twice for all topologies. The efficiency of scanning was 98.2% for all topologies, and 89% for two-prong events due to the loss of short tracks of recoil protons. Measurements on three projections were used for the geometrical reconstruction of events. The geometrical reconstruction and the following kinematical analysis have been carried out by an adapted version of the CERN program system based on the HIDRA library [12].

At definition of the momentum of the secondary particles and their errors, the spread of measured track points, the uncertainties of magnetic field and the influence of multiple scattering of particles have been taken into account. The mean relative errors of momentum measurements for surely identified protons (recoil protons) and $\pi^{\pm}$-mesons, without any restrictions on their track length, are $\langle \Delta P/P \rangle = 4.56\%$, and $\langle \Delta P/P \rangle = 2.65\%$, respectively. For the reliable separation of fragments by mass we studied secondary particles with measured length $L > 35$ cm in the chamber. For this type of selection, the mean relative errors in the measurements of the momentum did not exceed 3.5% for all charges. The absolute errors in measuring the azimuthal angle in the XOY plane proved to be $\langle \Delta\beta \rangle = (0.60 \pm 0.01)$ mrad, and $\langle \Delta\alpha \rangle = (1.5 \pm 0.02)$ mrad for the depth angle. In the definition of the inclusive cross-sections and mean multiplicities of fragments, the corrections taking into account the losses due to the above-mentioned restriction have been included.

3 Total and inelastic cross-sections of ^{16}O-p interactions

The total visible cross-section of ^{16}O-p interactions at 3.25 GeV/c ($\sigma_{\rm tot}^{\rm vis} = (375 \pm 9)$ mb) has been defined by double scanning of 20000 pictures. For elastic two-prong events, the estimation of losses connected with the chamber threshold momentum has been performed. The comparison of the multiplicity distributions from scanning and the following measurements showed an absence of systematic losses at the topologies of events. In this connection an estimation of the cross-sections was made by means of experimental data. We have defined the low limit value of the losses of the elastic two-prong events —(20 ± 2) mb— by extrapolating the distributions $\mathrm{d}\sigma/\mathrm{d}t$ for measured two-prong events to $|t| = 0$. By taking it into account, the total cross-section of ^{16}O-p interactions was found to be (395 ± 10) mb. Taking into account corrections connected with the scanning efficiency and part of the elastic scattering among two-prong events ($\approx 50\%$), we determined the cross-section of the inelastic ^{16}O-p interaction which proved to be $\sigma_{\rm in} = (334 \pm 6)$ mb.

4 The isotope composition of secondary fragments, and the topological cross-sections of fragmentation channels

In this section, the data on isotope composition of the secondary particles are presented. The part of fragments with charge $Z_{\rm f}$ was determined by the analysis of the distributions on the $X = Z_{\rm f}/p$ variable, where p is the fragment momentum in the laboratory frame.

The spectra of the multinucleon fragments on the X obtained for the definite charge of given fragments are well depicted by a sum of Gaussian distributions, corresponding to each isotope. The spectrum of particles with $Z_{\rm f} = 1$ and momentum $p > 2$ GeV/c is presented in fig. 1a. Three maxima can be observed from the figure, which correspond to the ^{1}H, ^{2}H, and ^{3}H isotopes of the hydrogen nucleus.

The proton spectrum is not symmetric with respect to the maximum, which may be explained by the contribution of at least two different mechanisms of fast protons formation; these protons are mainly formed as a result of intranuclear cascade, and "evaporation" processes at the break-up of the residual nucleus.

The spectrum of particles with $Z_{\rm f} = 1$ when restricting the emission angle by $\theta < 3.6^\circ$ *versus* the projectile direction is shown in fig. 1b. Such a restriction of the emission angle corresponds to protons with a transverse momentum $\leqslant 200$ MeV/c. It is seen that the proton part of the spectrum becomes symmetric. In the spectrum approximation by a sum of three Gaussian distributions (fig. 1b) corresponding to the contributions of ^{1}H, ^{2}H, and ^{3}H (χ^2/number of freedom degrees = 3), one obtains a good agreement when one assumes that the proton spectrum is depicted by a sum of two Gaussian functions with different widths (χ^2/number of freedom degrees < 1). The so-obtained fractions of hydrogen isotopes are presented in table 1. In the same table, the results obtained for fragments with $Z_{\rm f} = 2$–8, and the data calculated under CFEM with the above-mentioned restriction for singly charged fragments are presented. In table 1, ΔW is a statistical error of definition of the isotopes fraction.

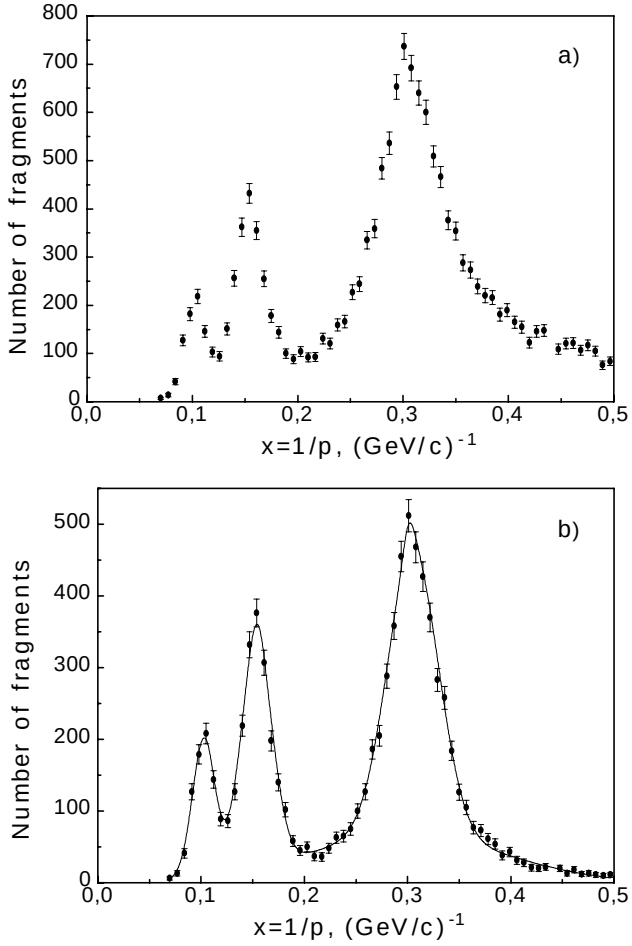

Fig. 1. Distribution of singly charged positive particles *vs.* $x = 1/p_{\rm f}$.

Let us consider table 2, where the inelastic cross-sections of the topological channels of fragmentation are presented. The charge composition of the fragments is indicated in brackets, and the corresponding cross-sections for the experimental and model data are shown below. The topology, $Z = 1$, corresponds to the channels without formation of multicharge fragments. It is seen from table 2 that the cross-section of the formation of doubly charged fragments accounts for a significant part of the inelastic cross-section.

It is interesting to mention the absence in the experimental data of the (44), (35), (233) topological channels where the total charge is equal to that of the initial nucleus.

In $(34 \pm 1)\%$ of the cases in the final state, two and more multicharge fragments are observed whose data are very close to those calculated under CFEM, $(36\pm1)\%$. But in experiment the observed cross-section of the formation of two and three helium nuclei is twice as much as that predicted by the model and the cross-section of formation of four doubly charged fragments differs significantly. Let us point out also that the probability of a doubly charged fragment accompanied by a heavier fragment is significantly greater in the model than in experiment.

Table 1. The fraction of different isotopes formed in ^{16}O-p interactions (%).

Z	A	Experiment		CFEM	
		W	ΔW	W	ΔW
	^{1}H	67.7		64.3	
1	^{2}H	22.9	0.6	24.6	0.4
	^{3}H	9.4		11.1	
	^{3}He	19.8		29.0	
2	^{4}He	79.7	0.9	68.5	0.5
	^{6}He	<0.5		2.5	
	^{6}Li	55.1		46.1	
3	^{7}Li	32.4	2.2	36.9	1.3
	^{8}Li	12.5		17.0	
	^{7}Be	56.6		55.7	
4	^{9}Be	38.3	3.0	16.4	1.2
	^{10}Be	5.1		27.9	
	^{10}B	48.2		42.5	
5	^{11}B	49.5	1.9	50.2	1.1
	^{12}B	2.3		7.3	
	^{10}C	3.5		16.2	
	^{11}C	18.2		38.4	
6	^{12}C	52.2	1.5	19.8	1.1
	^{13}C	18.8		20.1	
	^{14}C	7.3		5.5	
	^{13}N	9.4		8.9	
7	^{14}N	42.1	1.2	47.7	0.8
	^{15}N	48.5		43.4	
	^{14}O	6.1		3.3	
8	^{15}O	66.2	1.5	93.5	0.9
	^{16}O	27.7		3.2	

5 Formation of light (^{1}H ^{2}H ^{3}H ^{3}He) fragments

In this section the results of the study of the mechanisms of light-fragments formation with masses $A_{\rm f} \leqslant 3$ are presented.

In order to definitely identify the fragments by mass, we introduced the following momentum regions: $P = (4.6$–$7.8)$ GeV/c for ^{2}H, $P > 7.8$ GeV/c for ^{3}H nuclei, and $P < 10.8$ GeV/c for ^{3}He. The singly charged positive relativistic particles with $1.5 < P < 4.6$ GeV/c were identified as protons.

5.1 Mean multiplicities and inclusive cross-sections

In table 3, the mean multiplicities $\langle n_{\rm f} \rangle$ and the inclusive cross-sections $\sigma_{\rm in}$ of light-fragments (^{1}H, ^{2}H, ^{3}H, and ^{3}He) formation are presented.

It can be seen from table 3 that the inclusive cross-sections for the formation of "mirror" ^{3}H and ^{3}He nuclei are the same, within statistical errors.

Table 2. Inelastic cross-sections of oxygen nuclei fragmentation (mb).

Topology	$(Z = 1)$	(2)	(22)	(222)
Experiment	6.43 ± 0.46	23.58 ± 0.88	36.44 ± 1.10	31.27 ± 1.02
CFEM	5.19 ± 0.28	15.03 ± 0.48	19.69 ± 0.55	12.42 ± 0.43
Topology	(2222)	(23)	(24)	(25)
Experiment	3.51 ± 0.34	11.53 ± 0.62	6.66 ± 0.47	7.45 ± 0.50
CFEM	0.29 ± 0.07	13.83 ± 0.46	17.35 ± 0.51	20.02 ± 0.50
Topology	(26)	(223)	(224)	(233)
Experiment	10.14 ± 0.58	3.11 ± 0.32	0.93 ± 0.18	-
CFEM	23.32 ± 0.59	3.35 ± 0.23	1.06 ± 0.13	0.05 ± 0.03
Topology	(3)	(33)	(34)	(35)
Experiment	5.29 ± 0.41	1.26 ± 0.20	0.66 ± 0.15	-
CFEM	12.49 ± 0.44	2.50 ± 0.19	2.81 ± 0.21	0.15 ± 0.06
Topology	(4)	(44)	(5)	(6)
Experiment	5.60 ± 0.43	-	16.46 ± 0.73	54.16 ± 1.34
CFEM	13.09 ± 0.45	0.71 ± 0.11	21.39 ± 0.57	47.54 ± 0.85
Topology	(7)	(8)		
Experiment	65.35 ± 1.47	46.70 ± 1.24		
CFEM	75.51 ± 1.01	29.16 ± 0.67		

Table 3. Mean multiplicities $\langle n_{\rm f} \rangle$ and inclusive cross-sections $\sigma_{\rm in}$ of light-fragments (^{1}H, ^{2}H, ^{3}H, and ^{3}He) production.

	Fragment type			
	^{1}H	^{2}H	^{3}H	^{3}He
$\langle n_{\rm f} \rangle$	1.525 ± 0.017	0.350 ± 0.004	0.125 ± 0.001	0.126 ± 0.001
$\sigma_{\rm in}$ (mb)	549.0 ± 6.1	126.0 ± 1.4	45.0 ± 0.4	45.4 ± 0.4

Let us examine the correlations between the multiplicities of secondary particles and the formation of ^{3}H, or ^{3}He nuclei. Table 4 shows that the mean associative multiplicities of singly (except for protons) and doubly charged particles, and also of multiply charged fragments with a charge $Z \geqslant 3$, in semi-inclusive reactions in which a single ^{3}H, or ^{3}He nucleus is emitted, are practically the same.

It is seen from table 4 that the mean associative multiplicities of light particles with $2 \leqslant A \leqslant 4$, within statistical errors, proved to be the same for both nuclei. The experimental results show that the angular spectra are also coinciding for "mirror" ^{3}H and ^{3}He nuclei with the following mean emission angles and dispersions: $\langle \theta(^3\mathrm{He}) \rangle = (1.43 \pm 0.03)^\circ$, $\sigma(\theta(^3\mathrm{He})) = 1.03^\circ$, and $\langle \theta(^3\mathrm{H}) \rangle = (1.42 \pm 0.04)^\circ$, $\sigma(\theta(^3\mathrm{H})) = 1.02^\circ$.

The differences observed at associative multiplicities of proton fragments are probably due to the influence of the charge conservation law.

We may probably expect similar effects in reactions of projectile nucleus break-up into fragments, in which, nuclei with masses $A_{\rm f} > 3$ are absent. Such events may be assigned to reactions of oxygen nucleus complete break-up, because there are no fragments that can be formed from α-clusters among them. The total cross-section of the above-mentioned channels proved to be 15.54 ± 0.78 mb.

In table 5 the mean multiplicities of fragments (^{1}H, ^{2}H, ^{3}H, ^{3}He, and π^--mesons) are presented in different complete–break-up channels. It is seen that in oxygen nucleus complete break-up into fragments with mass numbers $A_{\rm f} \leqslant 3$, the mean multiplicities of "mirror" ^{3}H, and ^{3}He nuclei appeared to be as close as in the inclusive ^{16}O-p reactions. When comparing the features of the complete–break-up channels with the absence of one of the "mirror" fragments with $A_{\rm f} = 3$ ($n(^3\mathrm{He}) = 0$, and $n(^3\mathrm{H}) = 0$ channels), we found that not only the mean multiplicities of ^{3}H and ^{3}He nuclei, but also the probabilities of those channels were identical. The mean multiplicities of ^{2}H nuclei are also the same in these channels. Such an isotope symmetry also takes place in events with production of both "mirror" nuclei ($n(^3\mathrm{H}) \geqslant 1$, $n(^3\mathrm{He}) \geqslant 1$).

Table 4. The mean associative multiplicities of fragments in channels with "mirror" nuclei (^{3}H and ^{3}He) formation.

Particle type	Type of "mirror" nucleus	
	^{3}H	^{3}He
^{1}H	3.06 ± 0.06	2.50 ± 0.05
^{2}H	0.71 ± 0.02	0.71 ± 0.02
^{3}H	1.0	0.29 ± 0.01
^{3}He	0.28 ± 0.01	1.0
^{4}He	0.85 ± 0.03	0.86 ± 0.03
$A(Z \geqslant 3)$	0.25 ± 0.02	0.21 ± 0.02

Table 5. Mean multiplicities of light fragments, and π^--mesons in different channels of the oxygen nucleus complete break-up.

Channels	Part of events (%)	$\langle n(^1\mathrm{H})\rangle$	$\langle n(^2\mathrm{H})\rangle$	$\langle n(^3\mathrm{H})\rangle$	$\langle n(^3\mathrm{He})\rangle$	$\langle n(\pi^-)\rangle$
$A_\mathrm{f} \leqslant 3$	100	3.78 ± 0.07	1.40 ± 0.07	0.82 ± 0.04	0.83 ± 0.04	0.50 ± 0.03
$N(^3\mathrm{He}) = 0$	44.2 ± 3.4	3.93 ± 0.11	1.76 ± 0.13	1.08 ± 0.08	-	0.43 ± 0.03
$N(^3\mathrm{H}) = 0$	41.4 ± 3.3	3.58 ± 0.09	1.70 ± 0.13	-	1.11 ± 0.09	0.58 ± 0.05
$N(^3\mathrm{He}) \geqslant 1$ $N(^3\mathrm{H}) = 0$	28.5 ± 2.7	3.54 ± 0.14	1.49 ± 0.14	-	1.61 ± 0.15	0.53 ± 0.05
$N(^3\mathrm{H}) \geqslant 1$ $N(^3\mathrm{He}) = 0$	29.6 ± 2.8	4.67 ± 0.15	1.59 ± 0.15	1.55 ± 0.14	-	0.32 ± 0.03
$N(^3\mathrm{H}) \geqslant 1$ $N(^3\mathrm{He}) \geqslant 1$	29.0 ± 2.7	3.65 ± 0.13	0.84 ± 0.08	1.25 ± 0.12	1.27 ± 0.12	0.58 ± 0.05

It can be seen from table 5 that the π^--mesons mean multiplicity depends on the charge of fragments with $A_\mathrm{f} = 3$. It is significantly greater in events with ^{3}He formation than in those with ^{3}H. It may be explained in a simple way. The process of inelastic oxygen-nucleus–neutron charge exchange ($\mathrm{n} \to \mathrm{p} + \pi^-$) is the main source of π^--mesons formation at energies close to 1 GeV. Due to the above-mentioned fact, the residual compound nucleus in events with relatively fast π^--meson formation will be, on average, proton excessive, and thus may cause the increase of ^{3}He production probability.

The similarity of all presented characteristics of the ^{3}H and ^{3}He mirror nuclei indicates that these nuclei are apparently formed under identical physical conditions. The observed behaviour of isospin doublets cross-sections can be probably explained under the assumption that the Coulomb forces do not influence the formation of the observed fragments, and no additional charge is transferred to the residual excited nucleus.

It is interesting to note that a similar effect is observed in emissions of "mirror" nuclei with $A = 7$ (^{7}Li, ^{7}Be). The inclusive cross-sections of "mirror" nuclei formation with $A = 7$ (^{7}Li, ^{7}Be) were also the same within statistical errors:

$$\sigma_\mathrm{incl}(^7\mathrm{Li}) = 9.3 \pm 0.5 \text{ mb}, \quad \sigma_\mathrm{incl}(^7\mathrm{Be}) = 9.1 \pm 0.5 \text{ mb}.$$

5.2 Energy and angular spectra

Let us consider the energy and angular properties of the ^{1}H, ^{2}H, ^{3}H, and ^{3}He fragments. Their inclusive and energy spectra are presented in the antilaboratory frame that is, the projectile rest frame. In this reference frame, the kinetic energy of the identified few-nucleon nuclei with $A = 2, 3$ does not exceed 200 MeV. We imposed the same restriction on the kinetic energies of protons classified as fragments. As soon as this selection is applied, the π^+-mesons admixture to singly charged positive particles can be neglected.

The invariant structure function $f(T) = E\mathrm{d}^3\boldsymbol{\sigma}/\mathrm{d}\mathbf{p}^3$ of protons with respect to their kinetic energies T, along with CFEM calculations, are shown in fig. 2. It is seen from the figure that the experimental spectrum is divided into two regions characterised by different slopes. In the region $T < 20$ MeV the spectrum decreases fast as the energy increases, and in that with $T > 20$ MeV the spectrum becomes flatter approaching an exponential shape. The model calculations, on the whole, show a similar be-

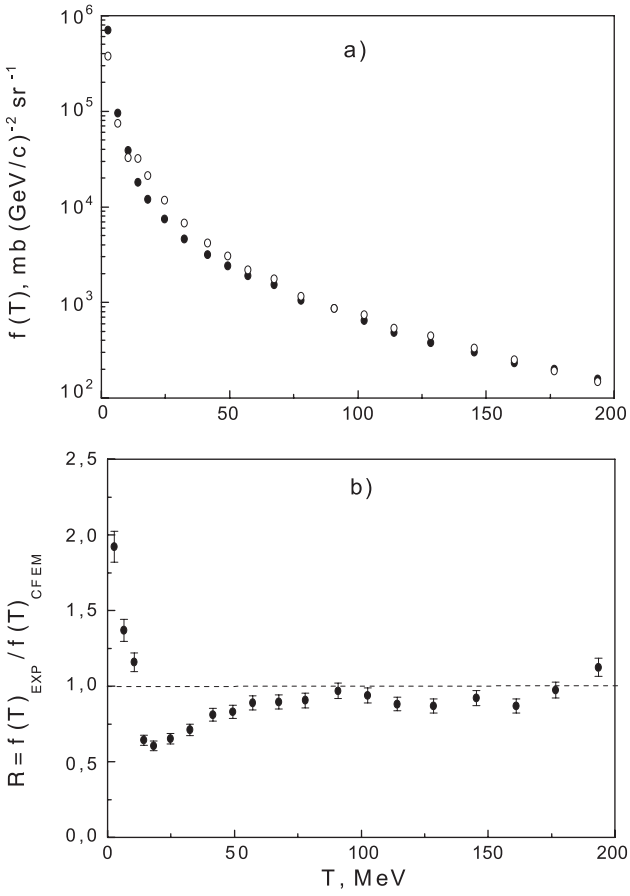

Fig. 2. Invariant structure function of protons as a function of kinetic energy $f(T)$ (a); and its ratio to CFEM calculations (b).

haviour. Herewith, in the region $T > 50$ MeV, where the products of intranuclear cascade dominate, CFEM depicts satisfactorily the experimental data. On the other hand, there are differences between the model and experiment in the region $T < 20$ MeV. Figure 2b shows them more clearly.

It is seen from this figure that in the model the cross-section of the low-energy protons is significantly smaller than in experiment. There are also discrepancies in the transition region $20 < T < 50$ MeV. Since in the kinematical region $T < 20$ MeV, the decisive contribution is given by the Fermi break-up in the model, the obtained result, probably, points out that the contribution of the "evaporation" processes (before the equilibrium stage) should be additionally taken into account in the CFEM.

Let us now proceed to analyse the experimental data of ^{2}H, ^{3}H, and ^{3}He formation. The distributions of the invariant structure function $f(T)$ and the corresponding model calculations are given in fig. 3a, b, c. As is seen from the figure, the experimental spectra of ^{2}H, ^{3}H, and ^{3}He in comparison with those of the proton show a flatter slope, but are also divided into two regions: $T \leqslant 20$ MeV, and $T > 25$ MeV. The model data behaviour is different from that of the experiment. Herewith, as is seen from fig. 3, in the low-energy region $T \leqslant 20$ MeV the CFEM satisfactorily agrees with experiment. As to the fast fragments ($T > 25$ MeV), there are differences between model and experiment, which augment as the kinetic energy increases. This fact, probably, may be due to the presence of the supplementary processes of the fast fragments formation which is not counted in the model. In this kinematical region, as it is known, the coalescence of cascade nucleons with small relative momenta may be due to this supplementary mechanism [15].

To estimate the contribution of this process, the following calculations were carried out within the coalescence model. Within the coalescence model [16], the cross-section for the production of fragments with mass number A_f is expressed in terms of the cross-section for proton production as

$$E_A \mathrm{d}^3\boldsymbol{\sigma}_A/\mathrm{d}\mathbf{p}_A^3 = C_A(E_\mathrm{p}\mathrm{d}^3\boldsymbol{\sigma}_\mathrm{p}/\mathrm{d}\mathbf{p}_\mathrm{p}^3)^A, \qquad (5.1)$$

provided that the distinction between the proton and neutron spectra is disregarded. Here p_p is the proton momentum, $p_A = A_\mathrm{f} \times p_\mathrm{p}$, C_A is the coefficient of coalescence which depends only slightly on the target mass and which is independent of the projectile energy and fragment emission angle [17].

The results of the corresponding calculations are shown by the solid curves in fig. 3, where the proton spectrum from the present experiment was used. The coefficient C_A was determined by fitting experimental data in the region $T \geqslant 75$ MeV. It can be seen that, in this region, the spectra of light fragments agree fairly well with the predictions of the coalescence model. A comparison of the fragment spectra with the predictions of the two different models (CFEM and coalescence model) reveals that we observe at least two sources of light nuclei. Of these, one is a residual thermalized excited nucleus decaying via the Fermi break-up mechanism. The other one is a process of the coalescence of fast nucleons formed at intranuclear cascade.

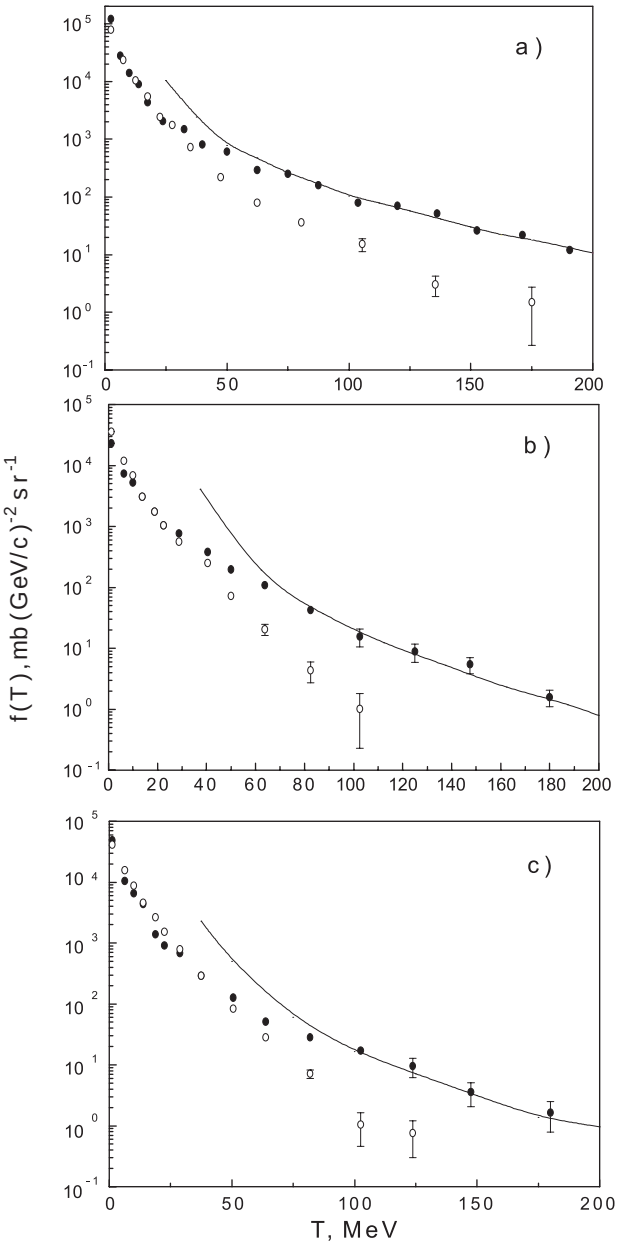

Fig. 3. Invariant structure function of light fragments as a function of kinetic energy $f(T)$. (• Experiment, ◦ CFEM, solid line: simulation accounts (see text); a) ^{2}H, b) ^{3}H, c) ^{3}He.)

As was mentioned above, the data of this experiment point out that the physical conditions of the "mirror" nuclei (^{3}H and ^{3}He) formation in proton interactions with the doubly magic ^{16}O nucleus are the same. Besides, the inclusive cross-sections, the angular spectra and the mean multiplicities of the ^{2}H and ^{4}He nuclei associated with the production of these nuclei also take up the same values. The identity of the invariant cross-sections distributions of the "mirror" nuclei with $A = 3$, as is seen from fig. 3, confirms this conclusion.

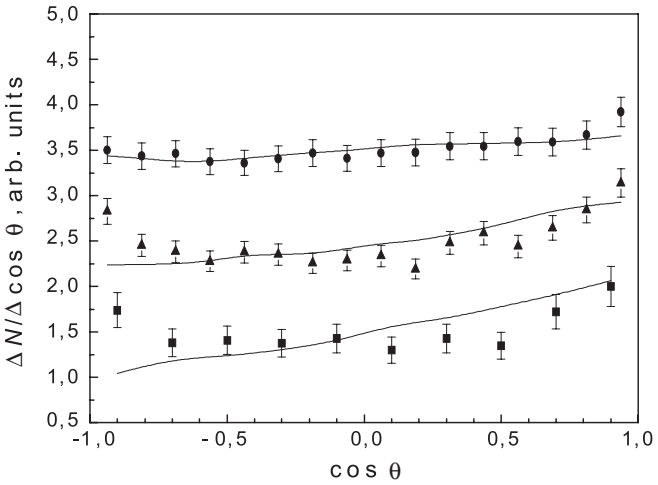

Fig. 4. The angular distribution of light fragments in the antilaboratory system. (• ^{1}H, ▲ ^{2}H, ■ ^{3}H $+^{3}$ He, solid line: CFEM.)

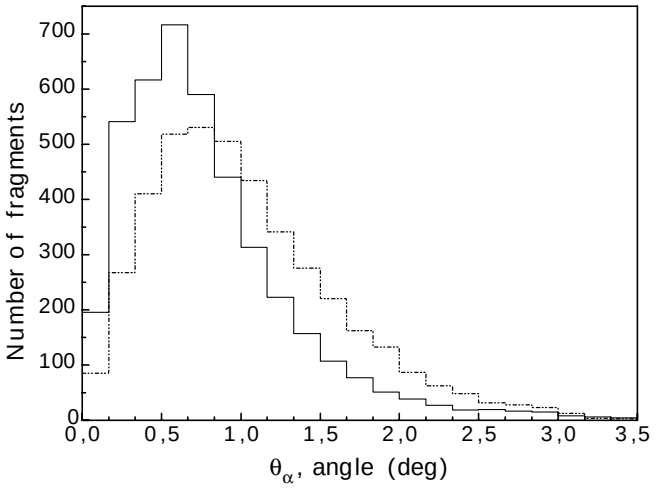

Fig. 5. The angular distribution of α-particles. (Solid histogram: experiment, dashed histogram: CFEM.)

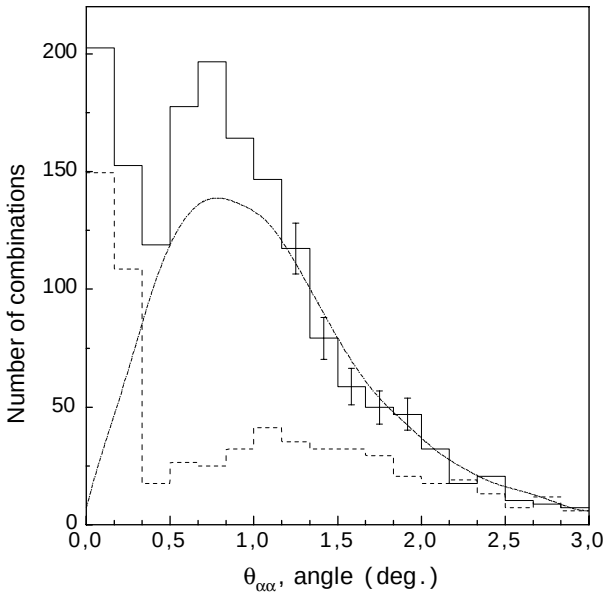

Fig. 6. Distribution of angles between α-particles. (Solid line: experiment, dash-dotted line: CFEM, dotted line: background.)

Let us consider the angular distributions of the low-energy ($T < 10$ MeV per nucleon) fragments ^{1}H, ^{2}H, ^{3}H, ^{3}He, which are presented in fig. 4 (taking into account the identity of the angular features of ^{3}H and ^{3}He nuclei, we associated the corresponding data in fig. 4). These distributions, on the whole, are not isotropic, having a minor forward asymmetry. The results of the CFEM calculations are also presented there (solid curves). The calculated data are normalised to the number of fragments in the experiment. It can be seen that the model reproduces well only the angular distributions of protons. The data for ^{2}H, ^{3}H, ^{3}He differ in experiment from those of CFEM. The most interesting feature in the behaviour of the angular dependences is that, for two- and three-nucleon fragments, there appear distinct effects indicating [18] that the residual nucleus undergoing fragmentation has a nonzero angular momentum: the cross-sections for these fragments tend to increase at the minimum and maximum emission angles.

6 Formation of the helium nuclei

6.1 The isotope composition of the doubly charged fragments

Let us consider the isotope composition of doubly charged fragments in different topological channels (see table 6). Fragments with $10.8 < p < 16$ GeV/c were identified as ^{4}He nuclei, and those with $p > 16$ GeV/c as ^{6}He.

The presented data allow us to mention the following singularities of the helium nuclei formation:

a) the model increases significantly the probability of ^{3}He nucleus formation and decreases that of ^{4}He;

b) the probability of ^{4}He (α-particles) nuclei formation in the channels with only doubly charged fragments formation increases with increasing their number. The same behaviour is also observed for topological channels, in which along with the helium nucleus, two- or four-charge fragments are formed;

c) ^{6}He, the heavy isotope of the helium nucleus, is observed only in (2) and (22) topologies (the detailed analysis of ^{6}He formation is presented below).

6.2 Formation of ^{4}He nuclei

As is well known, the fragmentation process, depending on excitation energy, may proceed via formation of short-lived unstable fragments or excited resonance states of the initial nucleus fragments [18]. In this section the results of the search of the intermediate states of the multinucleon systems fragmenting into α-particles, are presented.

Let us consider the angular distribution of α-particles by all possible topologies of their formation, which is

Table 6. Production of helium isotopes in the fragmentation channels (%).

Topolology	Fraction of He isotopes							
	$W(^3\mathrm{He})$	$W(^4\mathrm{He})$	$W(^6\mathrm{He})$	ΔW	$W(^3\mathrm{He})$	$W(^4\mathrm{He})$	$W(^6\mathrm{He})$	ΔW
	Experiment				CFEM			
(2)	28.9	69.6	1.5	2.2	28.7	58.9	12.4	1.9
(22)	21.9	77.4	0.7	1.1	30.8	65.9	3.3	1.0
(222)	15.2	84.8	–	0.8	22.7	76.5	0.8	0.9
(2222)	13.7	86.3	–	1.9	55.3	44.7	–	5.7
(23)	19.5	80.5	–	2.7	38.3	57.4	4.3	1.8
(223)	11.8	88.2	–	2.7	21.3	78.7	–	1.9
(224)	13.9	86.1	–	5.4	52.9	47.1	–	4.2
(24)	17.7	82.3	–	3.1	33.1	65.4	1.5	1.4
(25)	21.0	79.0	–	3.3	23.0	77.0	–	1.2
(26)	15.80	84.2	–	2.5	30.6	69.4	–	4.0

presented in fig. 5. Let us mention that the maximum value at $\theta_\alpha = (0.5 \pm 0.1)^\circ$ does not change with the topology, but the distribution width depends on the total charge of the fragments with $Z_\mathrm{f} \geqslant 2$; at $\sum Z_\mathrm{f} \geqslant 7$ it is 1.5 times narrower than at $\sum Z_\mathrm{f} < 7$. The maximal value of distributions and the mean emission angle of α-particles, calculated under CFEM, are slightly more: $\langle\theta\rangle_\mathrm{exp} = (0.82 \pm 0.02)^\circ$ and $\langle\theta\rangle_\mathrm{CFEM} = (1.02 \pm 0.01)^\circ$.

Let us consider the angular correlations between α-particles, which may give some information on their formation mechanisms. The distribution on the angle between α-particles is presented in fig. 6 (solid histogram). The substantial singularity of this spectrum is the irregular structure, *i.e.* the existence of two peaks, one of which is absent in the background distribution (solid curve). The background was obtained at random by a mixture of α-particles from different events by taking into account their multiplicities. The normalisation of the background and experimental distributions was fulfilled in the region $\theta_{\alpha\alpha} > 1$. There, as can be seen from fig. 6, a good agreement is observed.

It must be mentioned that such a structure is absent in the angular distributions between α-particles and fragments with $A_\mathrm{f} \leqslant 3$, and there is not a peak at the angles close to zero degree.

The narrow peak at the minimum relative angles has a $\sigma(\theta_{\alpha\alpha}) < 0.2^\circ$ width, which lies within the $\theta_{\alpha\alpha}$ measurement error, and therefore the true width of this peak is less than the above-mentioned value. It is natural to assume that if the emission of the pair of α-particles is correlated, then their relative momenta will be small. The most probable process causing the formation of such pairs can be the decay of the slightly excited system into two ^{4}He, for example, that of the unstable ^{8}Be nucleus. Taking the extreme angle between the correlated α-particles at $\theta_{\alpha\alpha} = 0.2^\circ$, one may estimate the maximal released energy E^* of the decay of the slightly excited system. It is obvious that the $\theta_{\alpha\alpha}$ will have the maximal value in the laboratory frame if the corresponding α-particles in their centre-of-mass system are emitted transversely to the direction of the decaying system. Then,

$$E^* = P_\perp^2 / M_\alpha,$$

where $P_\perp$ can be determined through the extreme angle $\theta_{\alpha\alpha} = 0.2^\circ$ and the mean value of α-particle momentum, $\langle P_\alpha \rangle$, in the laboratory frame:

$$P_\perp \approx \langle P_\alpha \rangle^* \sin(\theta_{\alpha\alpha}/2) = 22.6\ \mathrm{MeV}/c.$$

The value $E^* = 0.15$ MeV obtained by such a method is very close to the total kinetic energy transferred to the α-particles formed by the decay of the unstable ^{8}Be nucleus to its ground state (0^+), which equals 0.1 MeV. Other states of the ^{8}Be nucleus, such as first (2^+), and second (4^+) have higher excitation energies (3.04 and 11.4 MeV, respectively [19]), and cannot cause the appearance of narrow angular correlations between the formed α-particles.

The corresponding CFEM calculations are shown in fig. 6 (dashed histogram, in relative units). In the model, as was mentioned above, the contributions of the unstable nuclei decaying into α-particles were also taken into account ($^8\mathrm{Be} \to \alpha + \alpha$ and $^9\mathrm{Be} \to \alpha + \alpha + \mathrm{p}$). As can be seen from fig. 6, narrow correlations are available at the same angles both in the model and in experiment. Let us mention that the correlations in the production of two α-particles and a proton, expected in case of the unstable ^{9}B-nucleus formation, were not revealed.

An excess of the experimental spectrum over the background in the $\theta_{\alpha\alpha} = (0.5\text{–}1)^\circ$ angular interval can be explained by the formation of α-particles via the decay of the first excited state of ^{8}Be.

It is necessary to note that the observed pair correlations in α-particles formation at small relative angles may be partly due to the effects of identity and interactions in the final state [20].

Other unstable nuclei, such as ^{5}He and ^{5}Li, can also be a supplementary source of α-particles formation. The experimental data allowed us to estimate the cross-section of the formation of the unstable isotope ^{5}Li decaying into ^{4}He and a proton [21].

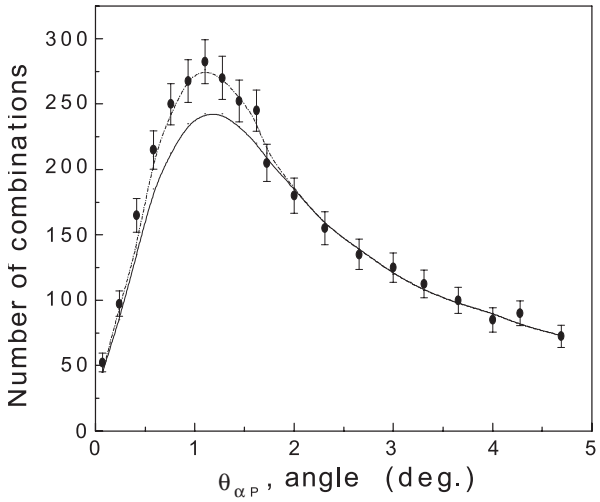

Fig. 7. Distribution of emission angles between α-particle and proton. (• Experiment, solid line: background, dash-dotted line: simulation accounts (see text).)

The events, having at least one ^{4}He nucleus and a fast proton, were selected from the total statistics for further analysis. Since projectile fragments are largely emitted with small transverse momenta and, hence, at small emission angles in the laboratory frame (of the order of few degrees), no event-by-event reconstruction of the decays $^5\mathrm{Li} \rightarrow \alpha +$ p is possible under the conditions of our experiment. For this reason, the yield of ^{5}Li nuclei was studied by comparing the distribution of the angle between α-particle and proton momenta, ($\theta_{\alpha\mathrm{p}}$), with the background distribution obtained with allowance for fractions of individual topological channels (recall that the angular distributions of fragments depend on these topological channels).

The background distribution was constructed by pairing at random an α-particle and a proton from different events. It should be noted that azimuthal correlations of kinematical origin might result from the break-up of an excited residual nucleus. In order to take them into account, the transverse momenta of the alpha-particle and the proton were determined preliminarily with respect to the total transverse momentum of all fragments detected in each event.

The results obtained in this way are illustrated in fig. 7. The background distribution (solid curve) was normalised to the number of events for $\theta_{\alpha\mathrm{p}} > 2^\circ$. It can be seen that the background distribution closely reproduces live events (black circles) at large angles, but that a significant excess over the background distribution is observed at small angles, where $\theta_{\alpha\mathrm{p}}$ correlations are expected in the case of ^{5}Li production in the ground state. The excess as a function of $\theta_{\alpha\mathrm{p}}$ is in good agreement ($\chi^2 < 0.5$) with the distribution calculated for the break-up of the ground-state ^{5}Li nucleus with allowance for a resonance width of $\Gamma = 1.5$ MeV. The sum of the background $\theta_{\alpha\mathrm{p}}$ distribution and the computer spectrum is represented in fig. 7 by the dashed curve.

Table 7. Mean values of the emission angle $\langle\theta\rangle$ and of the transversel momentum $\langle P_\perp\rangle$ for various helium isotopes in the topological channels with one and two doubly charged nuclei ($n(Z_\mathrm{f} = 2) = 1$, and 2).

Type of fragment	$\langle\theta\rangle$ ($'$)	$\langle P_\perp\rangle$ (MeV/c)
^{3}He	84 ± 2	234 ± 7
^{4}He	49 ± 1	185 ± 3
^{6}He	52 ± 8	296 ± 45
^{6}Li	44 ± 2	260 ± 16

Table 8. Cross-sections of the oxygen nucleus fragmentation into two and more multinucleon fragments.

Break-up channels	Cross-section (mb)	
	Experiment	CFEM
^{12}C ^{4}He	6.61 ± 0.66	2.49 ± 0.19
^{4}He ^{4}He ^{4}He ^{4}He	2.10 ± 0.38	0.015 ± 0.015
^{14}N ^{2}H	1.47 ± 0.29	0.62 ± 0.10
^{6}Li ^{4}He ^{4}He ^{2}H	0.27 ± 0.12	0.015 ± 0.015
^{10}B ^{4}He ^{2}H	0.16 ± 0.10	0.015 ± 0.015

The mean energy $E^* \approx 1.97$ MeV is actually released at $^5\mathrm{Li} \rightarrow \alpha +$ p nucleus decay in its ground state. In the rest frame of the ^{5}Li nucleus the momenta of the decay products will be equal to 54.4 MeV/c.

It is obvious that the maximal angle, $\theta_{\alpha\mathrm{p}}$, between α-particle and proton is obtained when they are emitted transversely to the ^{5}Li direction in the laboratory frame. This angle is $\theta_{\alpha\mathrm{p}} \approx 1.2^\circ$.

The cross-section for ^{5}Li formation proved to be $\sigma(^5\mathrm{Li}) = 8.4 \pm 0.5$ mb, which does not differ significantly from the excitation function values obtained previously by us for stable isotopes of lithium: $\sigma(^6\mathrm{Li}) = 12.0 \pm 1.1$ mb and $\sigma(^7\mathrm{Li}) = 9.6 \pm 1.0$ mb [13].

Such a significant production cross-section of unstable ^{5}Li nuclei may probably point out that this formation occurs through the coalescence of the α-cluster and the proton fragment of the initial nucleus.

6.3 Formation of ^{6}He nuclei

In the presented experimental data 13 events, containing one doubly charged fragment each, with mass number $A_\mathrm{f} = 6$, and momentum greater than 16.5 GeV/c, were found. The mean momentum of these fragments was found to be (19.6 ± 0.9) GeV/c, which is in good agreement with the value expected for ^{6}He nuclei. The production cross-section of this heavy helium isotope was estimated to be (0.60 ± 0.17) mb.

Let us consider some correlations between the production of particles and fragments from topological channels with ^{6}He production. There are no fragments with charge

Table 9. Characteristics of fragmentation channels with $\sum Z_{\rm f} = 8$.

Topology		σ (mb)	$\langle n_{\rm ch}\rangle$	$\langle n^-\rangle$	$\langle n_{\rm p}\rangle$	$W(^4{\rm He})$	$W(\sum A_{\rm f} = 16)$
	Exp.	3.51 ± 0.34	1.26 ± 0.10	0.13 ± 0.07	0.77 ± 0.05	86.5 ± 6.5	64 ± 11
(2222)	CFEM	0.29 ± 0.07	2.26 ± 0.25	0.63 ± 0.13	0.26 ± 0.15	44.7 ± 7.6	5 ± 5
	Exp.	0.93 ± 0.18	1.78 ± 0.22	0.39 ± 0.11	0.70 ± 0.11	> 85	0
(224)	CFEM	1.06 ± 0.13	2.31 ± 0.13	0.66 ± 0.09	0.44 ± 0.09	47.1 ± 5.8	0
	Exp.	10.14 ± 0.58	1.25 ± 0.05	0.13 ± 0.01	0.77 ± 0.05	84.4 ± 2.5	65 ± 6
(26)	CFEM	23.3 ± 0.6	1.80 ± 0.03	0.40 ± 0.02	0.55 ± 0.02	69.5 ± 1.2	11 ± 1

three or more in these channels, but there is one additional doubly charged particle in seven events, six of which involve ^{4}He nuclei.

Mean values of the emission angle $\langle\theta\rangle$ and of the transversel momentum $\langle P_\perp\rangle$ for various helium isotopes in the topological channels with one and two doubly charged particles ($n(Z_{\rm f} = 2) = 1$, and 2) are presented in table 7. For comparison, the corresponding values of ^{6}Li nuclei are also presented in the table. It can be seen that, within errors, $\langle\theta\rangle$ for ^{6}He agrees with the corresponding values for ^{4}He and ^{6}Li. This suggests that excited projectiles undergoing fragmentation may produce $A = 6$ nuclei via the coalescence of an α-cluster with two nucleons.

7 Break-up of ^{16}O into multinucleon fragments

Let us consider, in details, the channels of relativistic oxygen nuclei break-up into two and more multinucleon fragments with total number of nucleons $\sum A_{\rm f} = 16$.

The measured cross-sections for those channels of ^{16}O, where all constituent nucleons are carried away by the formed multinucleon fragments, are presented in table 8. The corresponding CFEM data are also shown in the table. It is seen from the table that, of all events in this category, more than 80% indicates only the even-even nuclei. The fraction of the multinucleon events with conservation of all nucleons in the (22) and (2222) (charges of fragments are indicated in brackets) topological channels amounts to about 2/3. Let us mention that the minimal excitation energy of oxygen nuclei needed for the formation of the above topologies amounts to 7.41 and 14.4 MeV, respectively. A few candidates for the final states ^{13}C^{3}He, ^{12}C^{2}H^{2}H, ^{11}C^{3}H^{2}H (one per channel) were also detected.

Let us consider the data of the oxygen nucleus fragmentation into multicharge fragments with total charge equal to that of the initial nucleus. Such break-up channels are obtained at small transfers in peripheral collisions, and as a consequence, they should be sensitive to the structural features of the oxygen nucleus, and to the clustering mechanisms of the nucleons in the slightly excited fragmenting nucleus.

The main features of the observed topological channels with $\sum Z_{\rm f} = 8$ ((224), (26), (2222) channels), are presented in table 9, where σ is the topological cross-section in mb, $n_{\rm ev}$ the number of events, $\langle n_{\rm ch}\rangle$, $\langle n^-\rangle$ and $\langle n_{\rm p}\rangle$ are the mean multiplicities of singly charged particles, π^--mesons and protons, respectively, $W(^4{\rm He})$ and $W(^{12}{\rm C})$ the fraction of the even-even helium and carbon nuclei isotopes production, $W(\sum A_{\rm f} = 16)$ is the fraction of events with conservation of all projectile nucleons in the multicharge fragments.

As can be seen from table 9, all of the presented experimental characteristics, excepting the cross-section, proved to be the same, within statistical errors, in the (26) and (2222) topological channels. In the channels with beryllium nuclei formation, the mean multiplicities of π^--mesons and singly charged particles are significantly greater than in others. The CFEM results differ significantly from the experimental ones, excepting the σ (224), in all characteristics presented in the table.

It is seen from the table that the isotope composition of the doubly charged fragments (the main fraction of which are α-particles ($> 84\%$)) is the same, within statistical errors, for all the three topologies. On the contrary, in the model, this composition depends on the topology, and the fraction of ^{3}He nuclei is significantly greater than in the experiment.

An analysis of the momentum spectra of fragments with $Z_{\rm f} = 4$, and 6 showed the following:

a) Four-charged fragments consist of ^{7}Be nuclei both in the model, and in the experiment. So, the total number of neutrons in the multicharge fragments, in the (224) channel, is always less than that in the initial projectile-nucleus.

b) The main part of six-charged fragments consists of the ^{12}C nucleus ($\approx 67\%$) but, in the model, the overwhelming part of the formed carbon nuclei consists of lighter isotopes ($\approx 83\%$).

The above-obtained isotope effects must probably reflect in the data of the multiplicities of singly charged particles. The formation of π^--mesons at conservation of the initial nucleus charge in secondary fragments, most probably, takes place in the inelastic collisions processes of the target-proton with one (or few) of the projectile-nucleus neutrons, which must result in the decrease of the

Table 10. The (26) channel cross-section with respect to $n_{\rm ch}$, the number of singly charged particles.

$n_{\rm ch}$	1	3	5
σ (mb)	8.94 ± 0.62	1.12 ± 0.20	0.09 ± 0.06

number of neutrons in the observed multicharge fragments in comparison with protons. Therefore, we may expect that in the (224) channel (containing always one or more neutron-deficient nuclei) the mean multiplicities of π^--mesons, and consequently, those of singly charged particles must be greater than in other channels, as is observed in the experiment. The existence of such a correlation is also seen from the CFEM data.

In the two other, channels (2222) and (26), identical by many features, the fragments formation process with the conservation of all nucleons of the initial nucleus takes place in about 2/3 of the events, while the fraction of such events amounts to approximately 10% in the model. In these events the fragments consist only either of α-particles, or of α-particle and ^{12}C. To identify the channels with ^{12}C nucleus production the momentum interval 37–41 GeV/c was chosen.

Let us consider in details the most statistically probable channel of break-up into multicharge fragments —the (26) topology.

The (26) channel cross-section with respect to $n_{\rm ch}$, the number of singly charged particles, is presented in table 10. It is seen that these fragments are accompanied by only one positive particle production in the overwhelming part of the studied channel; herewith, the fraction of protons with $P < 1.2$ GeV/c momentum amounts to nearly 80% .

The analysis of the momentum spectra showed that ^{4}He and ^{12}C nuclei were mainly formed in events with $n_{\rm ch} = 1$ and proton production (their cross-section amounts to (6.82±0.51) mb). In order to definitely identify fragments by mass, we introduced the following momentum regions: $Z = 2$ and $P = (10.8–15.0)$ for α-particles, $Z = 6$ and $P = (37.0–41.0)$ GeV/c for ^{12}C.

Furthermore, only the interactions with $P_{\rm p} < 0.5$ GeV/c and $\theta_{\rm p} > 70$, which might be referred to the following reaction, were considered:

$$^{16}{\rm O} + {\rm p} \to {\rm p} + {}^4{\rm He} + {}^{12}{\rm C}. \qquad (7.1)$$

The distribution of the difference between the azimuthal angles of the proton and α-particle $\Delta\varphi = |\varphi_{\rm p} - \varphi_\alpha|$ is strongly asymmetric with a significant maximum at $\Delta\varphi > 150^\circ$ (fig. 8) in these events. As to the azimuthal correlations in the production of the proton and the carbon nucleus, they are not evident.

One may consider the break-up of the oxygen nucleus into ^{4}He and ^{12}C nuclei as a result of:

1) quasi-elastic knock-out of an oxygen nucleus α-cluster by a proton;

2) diffractive excitation of the oxygen nucleus and its subsequent decay into the observed fragments.

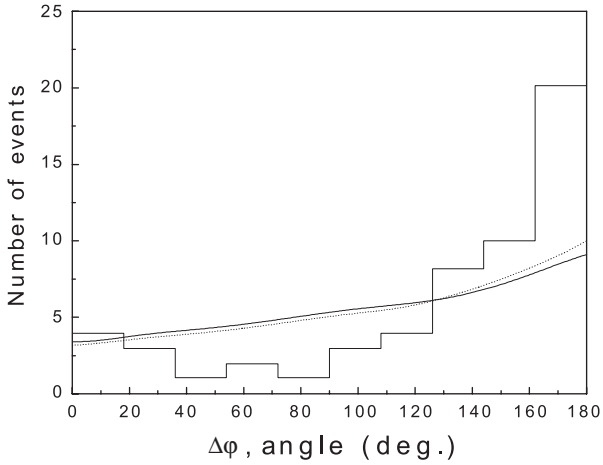

Fig. 8. Distribution of the difference between proton and α-particle azimuthal angles. (Histogram: experiment, solid line: phenomenological model, dotted line: CFEM.)

The existence at high energies of this special type of interaction —a collective excitation of a nucleus with the subsequent break-up into fragments— was theoretically predicted [22] (see also [23,24]). This process can proceed through the formation of the excited states of the oxygen nucleus with the following energy levels (MeV): $11.26(0^+)$, $11.6(3^-)$, $14.02(0^+)$, $16.8(4^+)$ and higher (the parity and spin are denoted in brackets), with the width of the resonance state greater than 0.1 MeV [19].

The obtained results show that the momentum and angular distributions of protons in this events have a maximum at small values of the momentum, $P_{\rm p} \approx 225$ MeV/c, and emission angle $\theta_{\rm p} \approx 81^\circ$, in the laboratory frame. This confirms that the process of the oxygen nucleus break-up into two fragments, ^{4}He and ^{12}C, has an "elastic" diffractive character. That is a scattering of a proton on the multinucleon system.

To check the first assumption, the calculations were performed in the frame of the following phenomenological model. An intermediate excited state of the initial nucleus was formed in the inelastic oxygen scattering on a proton. The mass of this nucleus was defined by the measured kinematical characteristics of a proton:

$$M(^{16}{\rm O}^*) = M(\alpha^{12}{\rm C}) = \left((E_{\rm Op} - E_{\rm p})^2 - (P_{\alpha{\rm C}} - P_{\rm p})^2\right)^{1/2}, \qquad (7.2)$$

where $P_{\alpha{\rm C}} = P_{\rm O} - P_{\rm p}$, $E_{\rm Op}$ is the total energy of initial particles, $P_{\rm O}$ and $P_{\rm p}$ are the momentum vectors of the projectile-oxygen and the secondary proton, respectively. The difference of this mass and the sum of α and ^{12}C masses is the break-up kinetic energy released:

$$\Delta E = M(\alpha^{12}{\rm C}) - M_\alpha - M_{^{12}{\rm C}}. \qquad (7.3)$$

The experimental distribution of ΔE has a form which is close to symmetric with respect to the mean value, $\langle\Delta E\rangle = (9.1 \pm 1.0)$ MeV, and with a mean square error of 5 MeV.

The calculations were implemented with the assumption that the excited nucleus break-up occurred with an isotropy in the (α^{12}C) rest frame in the following succession:

- the kinetic energies and momenta of α and ^{12}C fragments were calculated in this system;
- the emission angles of the fragments with respect to the direction of the (α^{12}C) system, and the azimuthal angles were simulated at random by the Monte Carlo method;
- the transfer to the laboratory frame was performed; to take into account the influence of the momentum and angle measurements errors, ΔP, $\Delta\alpha$, $\Delta\beta$ (errors of the momentum, depth, and flat angles measurements, respectively) were simulated at random by a normal law with dispersions defined by the experiment.

The obtained results are presented in fig. 8 (histogram: experiment, solid line: phenomenological model). The CFEM calculations are also presented in the figure (dotted curve). It is seen from the figure that calculations in the phenomenological and CFEM models are very close to each other, but they differ significantly from the experimental data in the region, $\Delta\varphi > 160°$. An observed substantial trend of the emissions of a proton and an α-particle in the opposite directions may strongly favour the mechanism of the quasi-elastic knock-out of the α-cluster from the ^{16}O projectile.

It is inferred from the presented data that, in the fragmentation of the oxygen nucleus into two fragments with conservation of all the nucleons of the initial nucleus, only a single (26) channel with even-even nuclei does occur.

8 Conclusion

The main conclusions of the present paper can be summarised in the following way:

1. The cross-sections of the topological channels and the isotope composition of fragments are determined. It is shown that the multifragment break-up of the oxygen nucleus is performed with the greatest probability, which main products are helium nuclei (about 80% of helium nuclei are α-particles). A significant part of α-particles is produced by the decay of the unstable short-lived ^{5}Li, and ^{8}Be nuclei. The same probabilities of formation of the "mirror" ^{3}H, ^{3}He, and ^{7}Li, ^{7}Be nuclei are observed.

2. From a comparison of the experimental data on the emissions of light fragments with the CFEM results, we may conclude that, besides Fermi break-up, there are other mechanisms of formation of light fragments. They are "evaporation" processes in the emission of slow protons in the oxygen rest frame, and the coalescence of the cascade nucleons resulting in the formation of the significant part of fragments with $A = 2$ and 3.

3. At the multifragment break-up of the oxygen nucleus into multinucleon fragments with conservation of all projectile nucleons, break-up channels into four α-particles or into two ^{12}C, and ^{4}He fragments occur with the greatest probability. The data agree satisfactorily with the mechanism of α-cluster knock-out, and the diffractive excitation of the nucleus as a whole.

In conclusion we would like to express our gratitude to the staffs of the JINR for the presented pictures from the 1-meter hydrogen bubble chamber and to A.S. Botvina, A.S. Iljinov and I.N. Mishustin for performing CFEM calculations.

References

1. J. Rufher, Phys. Rep. **125**, 129 (1985); W.G. Lynch, Ann. Rev. Nucl. Part. Sci. **37**, 493 (1986); ABGDDEZKKLMTTV Collab. (N.P. Andreeva), *Proceedings of the 20-th International Cosmic Ray Conference*, Vol. **5** (Nauka, Moscow) p. 61.
2. W.R Webber et al., Phys. Rev. C **41**, 520 (1990).
3. L.G. Moretto, G.J. Wozniak, Ann. Rev. Nucl. Part. Sci. **43**, 123 (1993).
4. J.P. Bondorf et al., Phys. Rep. **257**, 133 (1995).
5. A.S. Botvina et al., JINR Comm. P1-90-560 (1990).
6. Yu.P. Yakovlev, *Physics of Elementary Particles and Atomic Nuclei*, Vol. **14** (Energoatomizdat, Moscow, 1983) p. 1093.
7. E.O. Abdurachmanov et al., Yad. Fiz. **28**, 1304 (1978).
8. J. Povlot et al., Phys. Lett. B **233**, 16 (1989); V.A Karnaykhov et al., Yad. Fiz. **62**, 272 (1999).
9. A.S Botvina et al., Nucl. Phys. A **507**, 649 (1990).
10. A.S. Botvina et al., Preprint of the Institute of nuclear research of USSR Academy of Sciences, 126, Moscow (1989).
11. B.S. Aladashvili et al., JINR Comm. 1-7645, Dubna, 1973; B.S. Aladashvili et al., Nucl. Instrum. Methods **129**, 109 (1975).
12. Ya. Bolgansuren et al., Preprint of JINR, P10-89-40, Dubna, Russia (1989).
13. V.V. Glagolev et al., JETP Lett. **58**, 497 (1993).
14. V.V. Glagolev et al., JETP Lett. **59**, 336 (1994); Yad. Fiz. **58**, 2005 (1995).
15. V.D. Toneev et al., *Physics of Elementary Particles and Atomic Nuclei*, Vol. **17** (Energoatomizdat, Moscow, 1983) p. 1093.
16. F. Butler, C.A. Pearson, Phys. Rev. **129**, 836 (1963); A. Schwarzschild, C. Zupancic, Phys. Rev. **129**, 854 (1963).
17. S. Nagamiya et al., Nucl. Phys. **24**, 971 (1981).
18. V.S. Barashenkov, V.D. Toneev, *Interactions of High-energy Particles and Nuclei with Nuclei* (Moscow, Atomizdat, 1972).
19. F. Ajzenberg-Selove, Nucl. Phys. A **490**, 1 (1988).
20. G.I. Kopylov, M.I. Podgorezckiy, Yad. Fiz. **15**, 392 (1972); **18**, 656 (1973); **19**, 434 (1974); G.I. Kopilov, Phys. Lett. B **50**, 472 (1974).
21. V.V. Glagolev et al., Yad. Fiz. **63**, 575 (2000).
22. I.Ya. Pomeranchuk, E.L. Feynberg, *Reports of USSR Academy of Sciences*, Vol. **53**, p. 439 (1953).
23. V.V. Belaga et al., Yad. Fiz. **59**, 869 (1996).
24. F.A. Avetyan et al., Yad. Fiz. **59**, 110 (1996).